Specific features of acoustic emission of Ti alloys under plastic strain and fracture

Cite as: AIP Conference Proceedings **2167**, 020070 (2019); https://doi.org/10.1063/1.5131937
Published Online: 19 November 2019

A. A. Dmitriev, and V. V. Polyakov

Specific Features of Acoustic Emission of Ti Alloys under Plastic Strain and Fracture

A. A. Dmitriev[a)] and V. V. Polyakov[b)]

Altai State University, Barnaul, 656049 Russia

[a)] dmitriev@asu.ru
[b)] Corresponding author: pvv@asu.ru

Abstract. This paper investigates acoustic emission of annealed and unannealed Ti alloys under static tension. Unannealed Ti alloys have three distinctive AE peaks related to different stages of strain hardening. There is a significant difference in AE signal form and two peaks for annealed Ti alloys. Discrete wavelet transform is used to analyze the measured acoustic emission peaks quantitatively. Calculated informative parameters of acoustic emission allow establishing the relation between acoustic emission and mechanisms of plastic strain and rupture under loading of Ti alloy. Obtained results can be used to analyze acoustic emission testing results of Ti alloys.

INTRODUCTION

Titanium alloys are widely used for the manufacturing of core structural parts of modern technical equipment. They have very high tensile strength and toughness, corrosion resistance, and the ability to withstand extreme temperatures. Such properties explain the importance of titanium alloys when dealing with various external environments. Widespread use of titanium alloys necessitates the development of modern methods and techniques for testing loaded alloy materials. Acoustic emission technique (AET) has been used extensively to characterize damage mechanisms in loaded materials [1, 2]. However, the relation between acoustic emission (AE) signal and mechanisms of plastic strain in titanium alloys should be established beforehand to ensure the success of AET application. Despite numerous research efforts, experimental data are contradictory [3–7], and the relation mentioned above actually has not been established yet. The object of this paper is to reveal the relation between AE and physical deformation mechanisms using the wavelet-based analysis of AE signals proposed by authors in [8, 9].

MATERIALS AND TESTS

Mechanical tests are conducted on VT1-0 (Grade 2) titanium alloy specimens in their initial conditions and annealed specimens by applying static tension. Annealing has been done at 885°C for 25 min with further air cooling. Surface structures of specimens were analyzed by optical microscopy, and surface profiles were studied with atomic force microscopy. Specimens demonstrate their equiaxed grain structures with an average grain size of 15–20 μm (initial condition) and 50–70 μm (annealed). There are twinning bands in some grains of unannealed Ti specimens in their initial condition.

Strain hardening curves σ–ε obtained using experimental measurements of loading and elongation describe the mechanics of titanium alloy specimens (Fig. 1). Figure 1 shows the decrease of the ultimate tensile strength (UTS) and the increase of critical strain for annealed specimens.

AE signals, described by root mean square (RMS) voltages, were recorded simultaneously with measurements of loading and elongation. Piezoelectric transducers GT-301 with operational frequencies from 50 to 500 kHz were used to record AE signals with a sampling rate at 2.5 MHz. Calculated ratios of RMS voltages U_s obtained from the transducer to the idle state noise level U_n are plotted for unannealed and annealed Ti alloy specimens (Fig. 2).

Proceedings of the International Conference on Advanced Materials with Hierarchical Structure for New Technologies and Reliable Structures 2019
AIP Conf. Proc. 2167, 020070-1–020070-4; https://doi.org/10.1063/1.5131937
Published by AIP Publishing. 978-0-7354-1912-4/$30.00

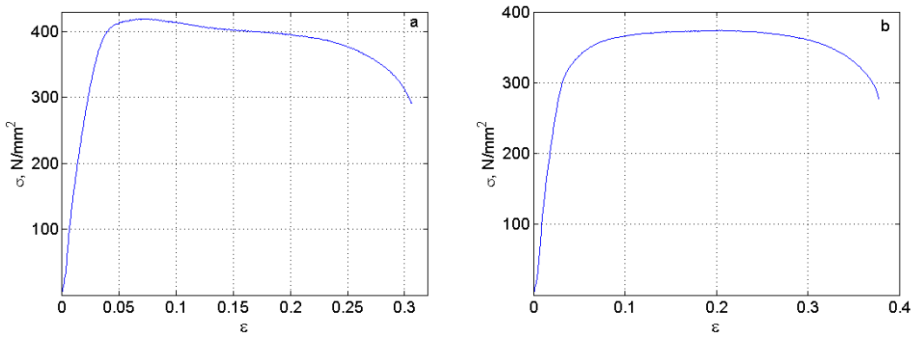

FIGURE 1. Strain hardening curves for Ti alloy specimens: (a) initial condition (unannealed), (b) annealed

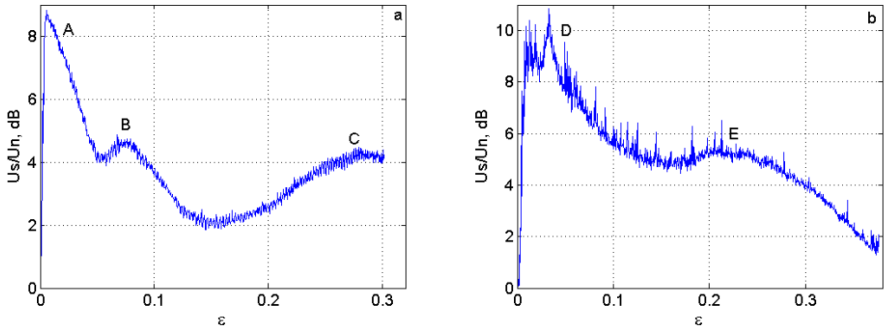

FIGURE 2. AE curves for unannealed (a) and annealed (b) Ti alloy specimens. Unannealed Ti alloy specimens: *A*—the first peak, *B*—the second peak, *C*—the third peak, annealed specimens: *D*—the first peak, *E*—the second peak

Figure 2 shows the qualitative difference between AE signals of unannealed and annealed Ti alloy specimens. There are three distinctive peaks with different amplitudes for unannealed Ti alloy specimens (Fig. 2a). The first peak *A* appears at the stage of linear hardening, the second peak *B* signifies the area of yield point and precedes the softening stage, the third peak *C* corresponds to a prefracture of a specimen. An annealed Ti alloy specimen have the oscillating AE curve with two wide peaks (Fig. 2b). Here, the first peak *D* covers the strain area that precedes the area of strong plastic flow. The second peak *E* represents the wide strain area at the stage of plastic flow. AE decreases monotonously in the areas of prefracture and fracture.

Revealed peculiarities of AE signals demonstrate the difference of plastic strain mechanisms which influence AE sources. Deformation structure of Ti alloy specimens has been analyzed to understand these differences. Figure 3 shows, as an example, the microstructure of a Ti alloy specimen in its initial condition according to the stages represented by three peaks of AE signals with strains of 0.02, 0.07, and 0.28, respectively. There are dislocation slip lines and small twins filling the grain area shown in Fig. 3a at small strains.

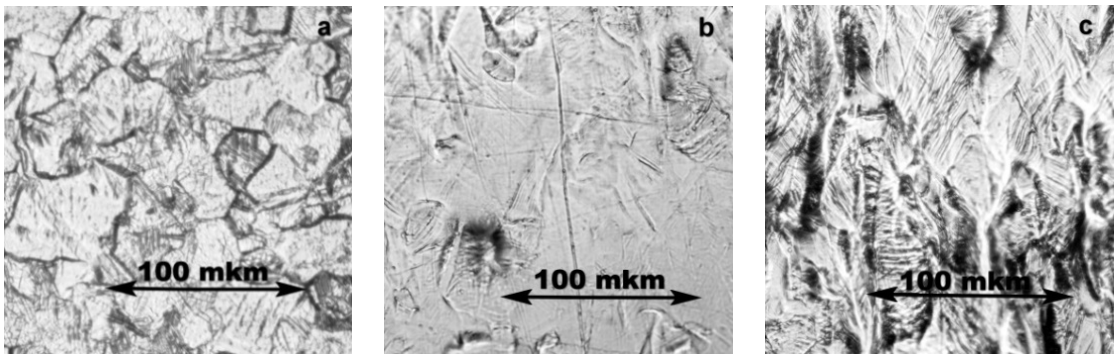

FIGURE 3. Ti alloy deformation structures. Strain ε = 0.02 (a), 0.07 (b), 0.28 (c)

Separate areas of non-uniform plastic strain and a multitude of dislocation slip lines, as well as individual large twins, can be found at the area of yield point (Fig. 3b) [10, 11]. Further increase of loading leads to strong fragmentation of a surface profile (Fig. 3c) and strong plastic effects around grain boundaries which cause relaxation of accumulated elastic strains at surface boundaries due to the appearance of microcracks.

Obtained experimental data allows establishing the relation between AE signals and plastic strain mechanisms. The first observed peak *A* of AE signals of unannealed and annealed specimens is likely to be caused by dislocation processes [4]. According to [5], small twins appeared during recrystallization from the melt are likely to contribute partially to the formation of the first peak. Strong AE signal oscillations and peak *D* widening for the annealed specimens should probably be related to the increase of grains sizes and more powerful dislocation processes caused by annealing. Dynamic of large twins formation due to significant plastic strain can explain the second peak *B* of AE signal of Ti alloy specimens in their initial condition [5, 6]. The third peak *C* is caused by the appearance and propagation of microcracks [7]. At the same time, it is extremely difficult to reveal predominant processes responsible for the appearance of the second AE peak *E* of annealed Ti alloy specimens. Therefore, quantitative matching of the second peak AE signals with the corresponding peak AE signals of unannealed specimens is done with the approach proposed by authors [8, 9] and used to study Al-Mg alloys.

PROCESSING RESULTS

Following the approach [8, 9], portions of AE signals describing peak areas are divided into blocks containing 10^7 instantaneous voltage values. Each block is processed by multilevel discrete wavelet transform (DWT) using the Daubechies wavelet [12, 13]. Calculated DWT coefficients are used as informative parameters of AE signals in each separate block and provide a quantitative representation of frequency and energy features of AE signals in peak areas [14].

Principal component analysis (PCA) is used to match the informative parameters for different peaks of AE signals. Calculated parameters for each block are treated as point coordinates in a multidimensional space. Latent dependencies are revealed by projection into lower dimension planes using principal components [15]. The first principal component is selected to stand for the maximum changes of the processed data, as well as the second and other principal components. This results in clustering of blocks with similar informative parameters. Further analysis is done using projections on planes of the leading principal components.

Processing results and projections on planes of the first and the second principal components PC1 and PC2 are presented in Fig. 4. Each point here represents a separate block of AE signals. Points related to the same peak are clustered together. Components PC1 and PC2 describe 85% of the processed data, so no other components are required [15]. Figure 4a shows the matching of the second peak *E* of AE signals of annealed specimens with the corresponding first peak *A* of AE signals of specimens in their initial condition. Figure 4b and 4c show the matching of the second peak *B* and the third peak *C*, respectively.

The closeness of two different clusters is estimated quantitatively using the minimum of Euclidean distance between two centers of clusters. For each cluster, PC1 and PC2 coordinates of points are averaged to produce the cluster center coordinates [16]. Euclidian distance is calculated using Eq. (1):

$$D_g(k,m)=\sqrt{\sum_{i=1}^{2}(k_i-m_i)^2}, \tag{1}$$

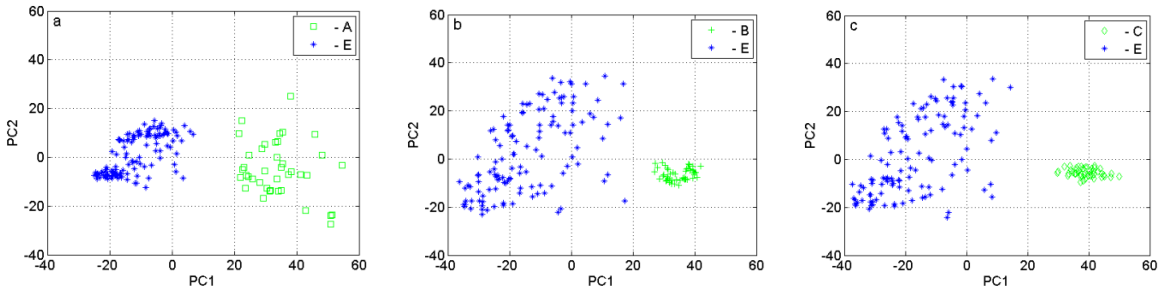

FIGURE 4. PCA analysis of AE peaks. Matching of the second AE peak of annealed specimens with the first (a), the second (b), and the third (c) AE peaks of unannealed Ti alloy specimens. Unannealed Ti alloy specimens: *A*—the first peak, *B*—the second peak, *C*—the third peak, annealed specimens: *E*—the second peak

TABLE. Calculated Euclidian distance between clusters centers

Cluster number	*A*	*B*	*C*
Distance *D* to the cluster *E*	33.12	30.13	35.60

where k_t—cluster center coordinates of each cluster corresponding to known AE peaks of unannealed Ti alloy specimens, m_t—cluster center coordinates of the cluster corresponding to the studied AE peak of annealed Ti alloy specimens, $D_g(k, m)$—Euclidian distance between the center of cluster E and centers of clusters *A*, *B*, *C*. Quantitative estimation of clusters closeness is shown in table.

The results show (Fig. 4 and table) that the points of clusters *A* and *C* are located farther from the geometric center of the cluster *E* than the points of cluster *B*. This signifies that informative parameters of AE peak *E* of annealed specimens are very close to the informative parameters of the second AE peak *B* of unannealed specimens. It allows this AE peak to relate to the twinning process.

CONCLUSION

This paper investigates acoustic emission of annealed and unannealed Ti alloys under static tension. It is demonstrated that unannealed Ti alloys have distinctive AE peaks related to dislocation and twinning processes of plastic strain and microcracking at the stage of fracture. There is a significant difference of AE signal form and fewer peaks for annealed Ti alloys.

AE signals are processed with multilevel DWT to uncover the mechanisms of plastic strain responsible for produced AE peaks. Calculated DWT coefficients are treated as informative parameters and processed further by PCA to cluster AE signals and reveal AE peaks with close informative parameters.

The proposed approach can be used to analyze acoustic emission testing results of Ti alloys.

ACKNOWLEDGMENTS

The work was carried out at the financial support of the RFFI in the framework of the grant No. 17-08-00914.

REFERENCES

1. G. D. Connolly, J. Li, and S. I. Rokhlin, NDT & E Int. **55**, 47–56 (2013).
2. A. N. Vshivkov, A. Yu. Iziumova, I. A. Panteleev, A. V. Ilinykh, V. E. Wildemann, and O. A. Plekhov, Eng. Fract. Mech. **210**, 312–319 (2019).
3. J. Kumar, S. Punnose, C. K. Mukhopadhyay , T. Jayakumar, and V. Kumar, Res. Nondest. Eval. **23**(1), 17–31 (2012).
4. A. V. Panin, V. E. Panin, Yu. I. Pochivalov, V. A. Klimenov, I. P. Chernov, R. Z. Valiev, M. S. Kazachonok, and A. A. Son, Phys. Mesomech. **5**(3–4), 125 (2002).
5. E. Z. Kayumova, V. V. Astanin, and A. A. Girfanova, Lett. Mater. **3**(3), 193–197 (2005).
6. N. V. Kamishanchenko, I. S. Nikulin, E. S. Kungurcev, and M. S. Kungurcev, Tech. Phys. Lett. **39**(10), 44–48 (2013).
7. P. I. Stoev and I. I. Papirov, Prob. Atom. Sci. Tech. **4**(16), 184–192 (2007).
8. A. A. Dmitriev, V. V. Polyakov, and A. A. Lependin, Lett. Mater. **8**(1), 33–36 (2018).
9. A. A. Dmitriev, V. V. Polyakov, and E. A. Kolubaev, Bas. Probl. Mater. Sci. **14**(4), 458–463 (2017).
10. V. I. Danilov, L. B. Zuev, and A. A. Zagumenniy, Fiz. Mezomekh. **9**(spec. iss.), 91–94 (2006).
11. I. O. Bolotina, V. I. Danilov, and A. A. Zagumenniy, Appl. Mech. Tech. Phys. **49**(3), 164–172 (2008).
12. S. A. Mallat, *Wavelet Tour of Signal Processing* (Academic Press, 2009).
13. Y. Ding, R. L. Reuben, and J. A. Steel, NDT&E Int. **37**(4), 279–290 (2004).
14. M. N. Shahri, J. Yousefi, M. Fotouhi, and M. A. Najfabadi, J. Compos. Mater. **50**(14), 1897–1907 (2016).
15. K. H. Esbensen, *Multivariate Data Analysis—In Practice* (CAMO Process AS, Oslo, 2002).
16. M. Kuhn and K. Johnson, *Applied Predictive Modeling* (Springer, 2013).